Spatial Resolution of Plasma Bubbles using Time-Delay Integration Images from ICON's Far-Ultraviolet Spectrographic Imager

Andrew Napiecek (andrewn7@vt.edu), Scott England

VIRGINIA TECH

Space @ Virginia Tech
Center for Space Science and Engineering Research

Introduction

One of ICON's main objectives is to measure the variability in the ionosphere and how disturbances from the lower atmosphere influence these processes. When the spacecraft is in darkness, the Far-Ultraviolet (FUV) Spectrographic Imager onboard captures FUV emissions primarily from the recombination of atomic oxygen ions. A key focus of imaging the nightside ionosphere is to capture the formation and growth of plasma bubbles. Plasma bubbles are instabilities that occur after sunset in the ionosphere due to a denser F-region existing above the "lighter" D and E regions that have started to recombine without constant ionization from the Sun. Plasma bubbles can disrupt radio transmissions and cause GPS range errors. The relatively low orbit of ICON and twelve second integration period necessitate a novel variable-range, motion-compensation technique to be implemented called Time-Delay Integration (TDI). Through simulated surfaces and model data, a variable-range TDI will be shown to have the resolution needed to observe the intricate structuring of plasma bubbles.

Time-Delay Integration

FUV emissions from recombining oxygen on the nightside ionosphere are relatively dim, therefore a twelve second integration period was needed to keep to the signal-to-noise ratio sufficiently low. This in combination with the ICON's nominal altitude of 575 km, results in significant motion blur at different rates across the image during integration. The TDI technique works by transforming the observed scene onto a surface that has constant linear motion. Then, images can be simply co-added together by linearly offsetting each successive image. A checker-board pattern, 1° x 1° in latitude and longitude, was projected onto a surface of tangent points and a sub-limb tangent height of 300 km above a spherical Earth to demonstrate this transformation. The greyed-out regions represent areas in the 256 x 256 pixel image where there is no data. The image is cut-off and rounded in the spacecraft view due to geometric distortions in the instrument's design.

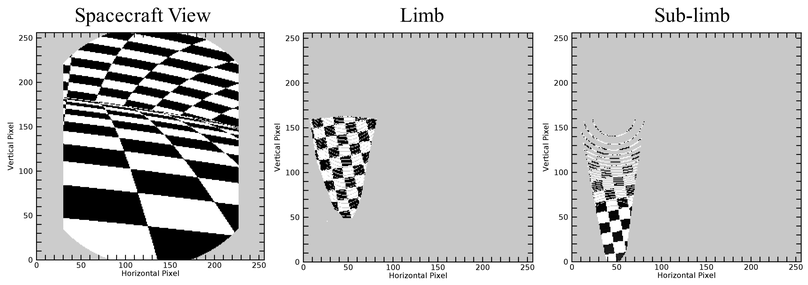

Figure 1: TDI transformation to surface with constant linear motion at -10° turret angle

Bands of missing data in the sub-limb and limb images are the result of round-off errors and subsequently those locations in latitude and longitude have no corresponding data in the spacecraft's field of view.

SAMI3 Model

The output from the SAMI3 model was used to simulate viewing a plasma bubble from ICON's FUV Imager. The high-resolution 'wedge' of the model containing a plasma bubble was mirrored six times, end-to-end, to eliminate any discontinuities, since the wedge only covers ~2° in longitude and the field of view of the FUV Imager is ~6° in longitude. Figure 2 shows a cross-section at 0° latitude of the mirrored SAMI3 model output data. I would like to thank Dr. Joe Huba for graciously allowing us to use the SAMI3 model data.

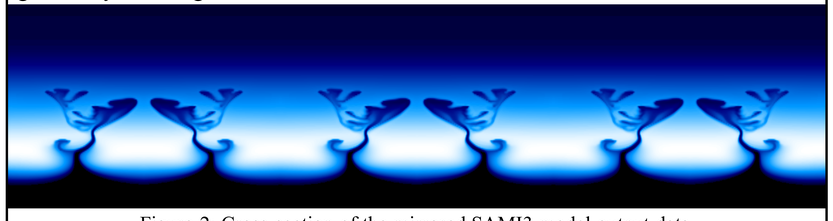

Figure 2: Cross-section of the mirrored SAMI3 model output data

TDI Plasma Bubble from SAMI3 Model

The SAMI3 model's output is density of electrons, cm^{-3}, and in order to convert the raw data to brightness values registered by the FUV instrument we will use Equation 1. This equation only accounts for FUV emissions from radiative recombination of O^+, excluding mutual neutralization of O^+ with O^- because it only accounts for a small fraction of the total brightness near sunset and it eliminates the added complications of sampling an addition model.

$$I_{RR} = \frac{1}{10^6}\int \alpha_{1356}(T_e)N_e[O^+]ds \qquad (1)$$

In Figure 3 a few cross-sectional profiles of electron density at different ranges from the spacecraft show the detailed structure of the plasma bubble. Electron density values are integrated along a line-of-sight using Equation 1 resulting in the final image seen at the FUV instrument.

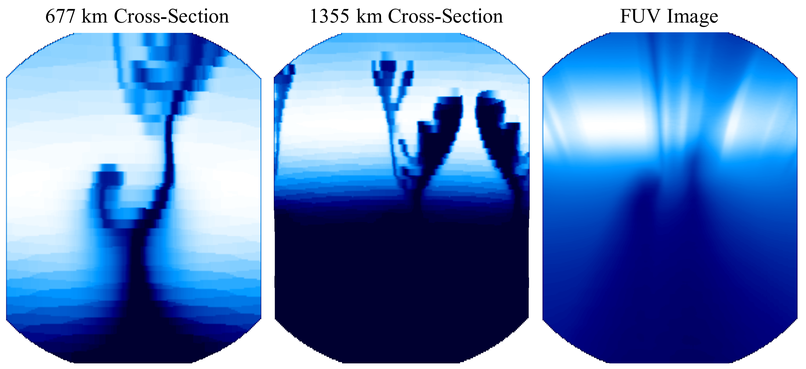

Figure 3: FUV Image formation from line-of-sight integrated electron densities

The SAMI3 model was sampled from a nominal spacecraft starting position of 0° latitude, 0° longitude, and 575 km altitude. The FUV images are then co-added together using the TDI technique for the 12 second integration period. Figure 4 shows the resultant limb and sub-limb images with and without the motion blur removed using the TDI process.

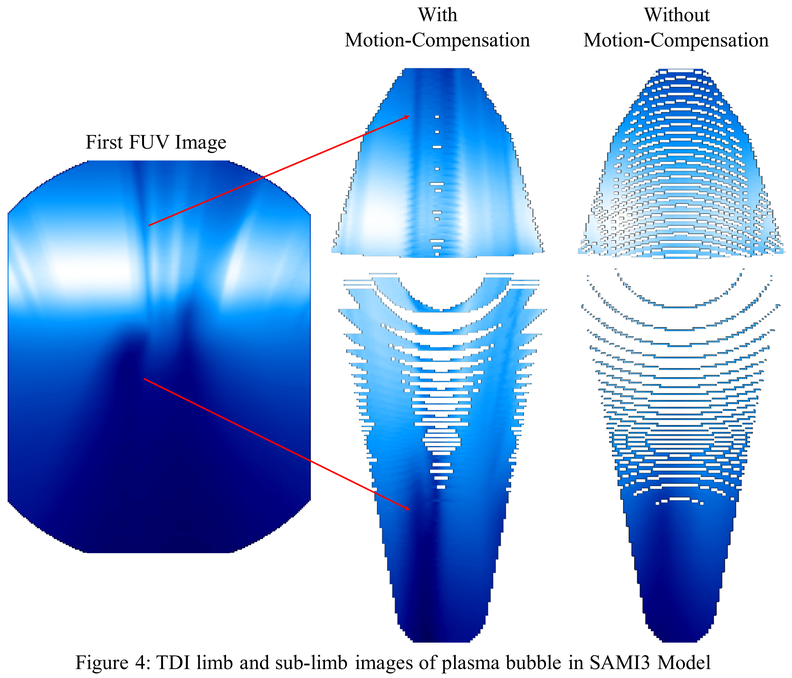

Figure 4: TDI limb and sub-limb images of plasma bubble in SAMI3 Model

Without compensation for the motion blur, the distinct two finger feature in the sub-limb image is non-existent. Similarly, in the limb image, detailed plasma gradients are smoothed out. These key detection features of plasma bubbles are shown in more detail in Figure 6.

Latitude and Longitude Profile Verification

For precise location of plasma bubbles seen by ICON's FUV Imager, a technique using ray-tracing and rotation matrices was used to determine the latitude and longitude of each pixel for any spacecraft position and instrument pointing. To verify each pixel has the correct latitude and longitude after it has gone through the TDI process, contour plots of latitude and longitude are presented and compared to latitude and longitude profiles from simulated 6-stripe altitude profile data previously produced for a separate data product. For this simulation the spacecraft is at 24.603° latitude, -46.769° longitude, and an altitude of 570.2 km at the mid-point of image integration.

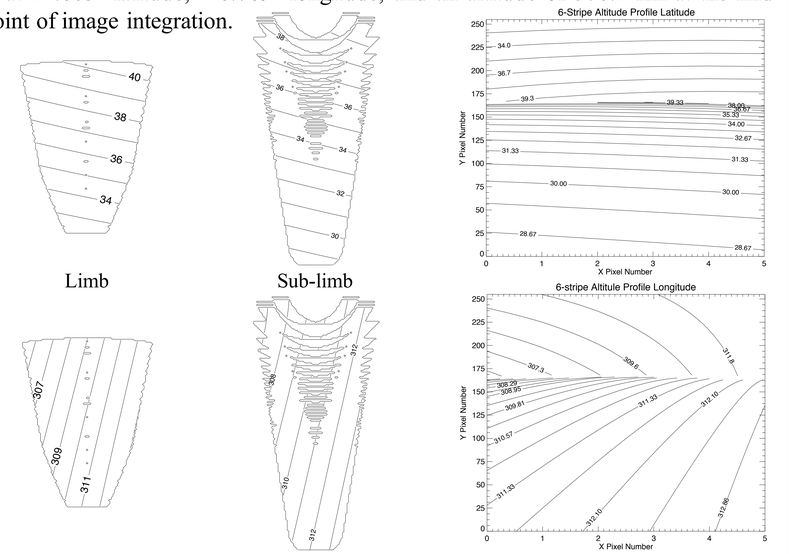

Figure 5: Limb and sub-limb latitude and longitude profile comparison

Plasma Bubble Gradient

Sharp plasma gradients on the edges of plasma bubbles are what cause interference of GPS and radio signals. To accurately model plasma bubbles in the future, we must determine the gradients in those we image accurately. We will look at the left wall of the plasma bubble in the limb image and the right wall of the plasma bubble in the sub-limb image. From Figure 6, it is clear the brightness gradient from the image with motion-compensation matches the true airglow gradient much better for both locations. All gradients were measured in rayleighs per pixel. For the left wall of the plasma bubble in the limb image, the true gradient is -66.17, with motion compensation it is -35.11, and without motion compensation it is -7.42. For the right wall in the sub-limb image, the true gradient is 21.6, with motion compensation it is 16.44, and without motion compensation it is 4.27.

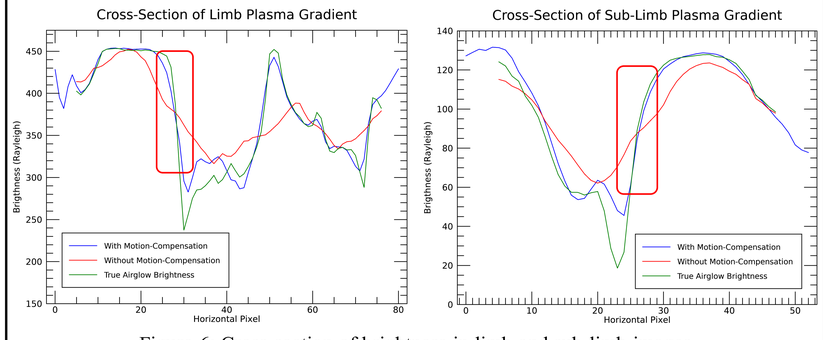

Figure 6: Cross-section of brightness in limb and sub-limb images

References

1. Wilkins, C.W., Mende, S.B., Frey, H.U. et al., Time-Delay Integration Imaging with ICON's Far-Ultraviolet Imager, Space Sci Rev (2017) 212: 715. https://doi.org/10.1007.s11214-017-0410-4
2. England, S. L., T. J. Immel, and J. D. Huba (2008), Modeling the longitudinal variation in the post-sunset far-ultraviolet OI airglow using the SAMI2 model, J. Geophys. Res., 113, A01309, doi:10.1029/2007JA012536.
3. Huba, J. D., G. Joyce, and J. Krall (2008), Three-dimensional equatorial spread *F* modeling, *Geophys. Res. Lett.*, 35, L10102, doi:10.1029/2008GL033509.
4. Mende, S.B., Frey, H.U., Rider, K. et al., The Far-Ultraviolet Imager on the ICON Mission, Space Sci Rev (2017) 212: 655. https://doi.org/10.1007/s11214-017-0386-0